

## Three-dimensional assemblies of graphene prepared by a novel chemical reduction-induced self-assembly method†

Lianbin Zhang,<sup>‡a</sup> Guoying Chen,<sup>‡ab</sup> Mohamed Nejib Hedhili,<sup>c</sup> Hongnan Zhang<sup>a</sup> and Peng Wang<sup>\*a</sup>

Received 6th August 2012, Accepted 13th September 2012

DOI: 10.1039/c2nr32157b

In this study, three-dimensional (3D) graphene assemblies are prepared from graphene oxide (GO) by a facile *in situ* reduction-assembly method, using a novel, low-cost, and environment-friendly reducing medium which is a combination of oxalic acid (OA) and sodium iodide (NaI). It is demonstrated that the combination of a reducing acid, OA, and NaI is indispensable for effective reduction of GO in the current study and this unique combination (1) allows for tunable control over the volume of the thus-prepared graphene assemblies and (2) enables 3D graphene assemblies to be prepared from the GO suspension with a wide range of concentrations (0.1 to 4.5 mg mL<sup>-1</sup>). To the best of our knowledge, the GO concentration of 0.1 mg mL<sup>-1</sup> is the lowest GO concentration ever reported for preparation of 3D graphene assemblies. The thus-prepared 3D graphene assemblies exhibit low density, highly porous structures, and electrically conducting properties. As a proof of concept, we show that by infiltrating a responsive polymer of polydimethylsiloxane (PDMS) into the as-resulted 3D conducting network of graphene, a conducting composite is obtained, which can be used as a sensing device for differentiating organic solvents with different polarity.

### Introduction

Graphene, a flat monolayer nanosheet of carbon atoms arranged in a two-dimensional (2D) honeycomb lattice, has attracted intense interest in recent years owing to its intriguing properties, such as high thermal and electronic conductivity, excellent mechanical strength, and high specific surface area.<sup>1–9</sup> An essential step to achieve advanced applications of graphene is to assemble individual graphene nanosheets into macroscopic materials, which translate the intriguing properties of graphene at the nanoscale into macroscopic devices.<sup>10,11</sup> For instance, freestanding graphene 2D macrostructures, such as membranes and paper-like thin films, could be obtained by layer-by-layer assembly,<sup>12–15</sup> Langmuir–Blodgett techniques,<sup>16,17</sup> vacuum-assisted filtration,<sup>18–21</sup> evaporation-induced self-assembly,<sup>22–24</sup> and direct chemical vapor deposition.<sup>25</sup> However, assembling the graphene nanosheets into the 2D macrostructures usually sacrifices the large accessible surface area of the graphene nanosheets, as the individual graphene nanosheets tend to aggregate and

restack due to strong  $\pi$ – $\pi$  interaction, hydrophobic interaction, and van der Waals force, which is undesirable for many applications. Working towards solving this problem and exploring further advanced applications, the preparation of three-dimensional (3D) graphene macrostructures, such as hydrogels,<sup>26–30</sup> aerogels,<sup>30–34</sup> and macroporous films,<sup>35,36</sup> has recently emerged as a research hotspot. These graphene-based 3D macrostructures generally have low density and highly porous structures with pore sizes as big as several tens of micrometers, which enable easy access and diffusion of ions and molecules throughout the highly porous structures.<sup>10,11,36</sup> Most importantly, these 3D graphene-based macrostructures effectively retain the accessible surface area of the individual graphene nanosheets, which is critical for achieving the maximum functionality of the graphene-based macroscopic materials and, as a result, they have found a lot of promising applications, such as catalysis,<sup>27,34,37</sup> sensors,<sup>28</sup> flexible electrically conducting nanocomposites,<sup>38</sup> energy storage and conversion,<sup>26,31,35,36</sup> and oil absorption and water purification.<sup>30,39</sup>

Existing methods for producing the 3D graphene macrostructures include template-directing method,<sup>32,35–37</sup> cross-linking method,<sup>27–29,33,40</sup> directed chemical vapor deposition,<sup>38,41–43</sup> and *in situ* reduction-assembly method.<sup>26,30,31,34,44</sup> The template-directing method uses ice crystals,<sup>32,37</sup> water droplets,<sup>35,36</sup> or colloidal particles<sup>32</sup> as the templates for the pore formation, and generally requires precise control over the amount of graphene used and subsequent template removal. The cross-linking method employs cross-linkers, such as sol–gel polymerization precursors,<sup>33</sup> polymers,<sup>28,29</sup> and ion linkages,<sup>27,40</sup> whose presence has unfortunately been found to lead to a decrease or a complete loss of the electrically

<sup>a</sup>Chemical and Life Sciences & Engineering Division, Water Desalination and Reuse Center, King Abdullah University of Science and Technology, Thuwal 23955-6900, Saudi Arabia. E-mail: peng.wang@kaust.edu.sa

<sup>b</sup>Department of Chemistry, Fudan University, Shanghai 200433, P. R. China

<sup>c</sup>Imaging and Characterization Laboratory, King Abdullah University of Science and Technology, Thuwal 23955-6900, Saudi Arabia

† Electronic supplementary information (ESI) available. See DOI: 10.1039/c2nr32157b

‡ These authors contributed equally to this work.

conducting properties of the thus-prepared 3D macrostructures. For the directed chemical vapor deposition method, 3D nickel foams are generally used as substrates, onto which graphene is deposited under high temperature conditions.<sup>38,41–43</sup>

Recently, it has been found that under a certain reducing environment, such as hydrothermal treatment<sup>26</sup> or the presence of a large amount of reducing agents,<sup>30,31,34,44</sup> graphene oxide (GO) can be reduced to graphene and spontaneously *in situ* assembled into a 3D macrostructure of the graphene. It is believed that as GO nanosheets are reduced in the reducing media, their surfaces become piece-wise hydrophobic due to their restored conjugated domains and diminishing oxygen-containing groups, which results in an increase in hydrophobic and  $\pi$ - $\pi$  interactions among the nanosheets, leading to a 3D random stacking of the graphene nanosheets.<sup>26,30</sup> The such-prepared 3D graphene macrostructures usually have pore sizes ranging from sub-micrometers to several micrometers. The *in situ* reduction-assembly method has many unique advantages, such as its facile procedure and easy scalability, but a high starting concentration of GO (*i.e.*, 2.0–4.0 mg mL<sup>-1</sup>) is generally required as shown in all existing reports for such a method to be successful.<sup>26,31,44</sup>

It was reported by the groups of Cheng and Lee independently<sup>45,46</sup> that halogenation agents, especially concentrated HI acid, could catalytically reduce oxygen-containing groups (*e.g.*, epoxy and hydroxyl groups) of GO, leading to a higher level of reduction of GO into high quality graphene compared with other reducing reagents. The proposed mechanism of HI for the improved reduction of GO is that, under acidic conditions, iodine can effectively replace oxygen-containing groups (*e.g.*, epoxy and hydroxyl groups) on GO to produce organohalides, which are good leaving groups from the carbon lattice, resulting in graphene.<sup>45</sup> However, the usage of a large amount of the highly toxic HI with high concentration makes the method not suitable for large-scale preparation of graphene-based materials.

With a clear aim of developing a more sustainable and greener reaction system for highly efficient GO reduction by iodine-based halogenation agents, herein, we report a novel and facile method to prepare 3D graphene macrostructures by reducing the GO suspension with a combination of low-cost, environmental-friendly reducing agents of oxalic acid (OA) and sodium iodine (NaI), which are rationally selected to replace the toxic HI. The reducing acid of OA together with iodine ions in the designed reaction system effectively reduces GO and very notably enables 3D graphene assemblies to be prepared from the GO suspension with ultralow concentrations (as low as 0.1 mg mL<sup>-1</sup>). The as-prepared 3D graphene assemblies show high conductivity, low density as well as good mechanical strength. Furthermore, as a proof of concept, we show that by infiltrating a responsive polymer of polydimethylsiloxane (PDMS) into the as-resulted 3D conducting network of graphene, a conducting composite is obtained, which can be used as a sensing device for differentiating organic solvents with different polarity.

## Experimental section

### Materials

Graphite powder (<20  $\mu$ m), sodium nitrate, potassium permanganate, hydrogen peroxide (30%), oxalic acid (OA), sodium

iodide (NaI), ethanol, acetone, and chloroform were purchased from Sigma-Aldrich. Sylgard 184 silicone elastomer base and curing agent were purchased from Dow Corning. All these chemicals were used as received. Deionized (DI) water purified in a Milli-Q (Millipore) system was used in all experiments.

### Synthesis of graphene oxide (GO)

GO nanosheets were synthesized from graphite by a modified Hummers' method.<sup>26,47</sup> Briefly, graphite powder (3.0 g) and sodium nitrate (1.5 g) were added to 70 mL of concentrated sulfuric acid, and the mixture was cooled using an ice bath to 0 °C. Under vigorous agitation, potassium permanganate (9.0 g) was slowly added into the above mixture, during which the temperature of the mixture was kept lower than 20 °C. Afterwards, the ice bath was removed and the reaction system was transferred to a 35–40 °C water bath and kept there for about 0.5 h. Then, a volume of 140 mL of water was added and the mixture was stirred for another 30 min. An additional 500 mL of water was added followed by a slow addition of 20 mL of H<sub>2</sub>O<sub>2</sub> (30%). The mixture was centrifuged at 3000 rpm to remove any aggregates, and then washed with 10% aqueous HCl solution four times to remove metal ions, followed by repeated washing with copious amount of water and centrifugation to remove the acid. The resulted aqueous suspension was sonicated for 1 h to make a GO suspension, followed by centrifugation at 3000 rpm to remove any large aggregates. The concentration of the GO suspension thus-prepared was 4.5 mg mL<sup>-1</sup>, which was determined by drying the suspension at 80 °C under vacuum for 24 h and then weighing the dried GO.

### Preparation of 3D assemblies of graphene

The 3D assemblies of graphene were prepared by the *in situ* reduction-assembly method using a combination of OA and NaI as the reducing agents. In brief, 20 mL of the GO suspension with a concentration of 0.1–4.5 mg mL<sup>-1</sup> was prepared, and then 0.5 g of OA and 1.0 g of NaI were added to the GO suspension. The mixture was sonicated for 10 min and then transferred to an oil bath at 90 °C for 12 hours without stirring. The resulted black cylinder of graphene hydrogel was washed with ethanol and water in a Soxhlet extractor for 24 h to remove residual impurities and then the wet hydrogels were freeze dried for 2 days to obtain graphene aerogel.

For the purpose of comparison, the reducing reaction of GO was also carried out using either 0.5 g OA or 1.0 g NaI alone, with the other conditions being the same.

### Preparation of graphene–PDMS composites

The graphene–PDMS composites were fabricated by infiltrating the previously prepared graphene aerogels with a PDMS precursor, containing the Sylgard 184 silicone elastomer base and curing agent in a 20 : 1 ratio, followed by degassing in a vacuum oven for 30 min and thermally curing at 60 °C for 12 h.

### Characterization

The morphology of the prepared graphene aerogels was characterized by scanning electron microscopy (SEM, FEI Company,

Quanta 600). X-ray diffraction (XRD) analyses were carried out on an X-ray diffractometer (Bruker D8 Advance), using Cu K $\alpha$  radiation (1.540598 Å). X-ray photoelectron spectroscopy (XPS) studies were carried out using a Kratos Axis Ultra DLD spectrometer equipped with a monochromatic Al K $\alpha$  X-ray source ( $h\nu = 1486.6$  eV) operating at 150 W, a multichannel plate, and a delay line detector under a vacuum of  $\sim 10^{-9}$  mbar. The survey and high-resolution spectra were collected at fixed analyzer pass energies of 160 eV and 20 eV, respectively. Fourier transform infrared (FTIR) spectra were recorded on a Nicolet iS10 (Thermo Scientific) Spectrometer. Raman spectra were recorded with a LabRAM HR800 (Horiba-Jobin Yvon) high resolution Raman spectrometer with laser excitation at 532 nm. N<sub>2</sub> sorption at 77 K was carried out with a Micromeritics Tristar II 3020 surface and porosimetry analyzer, and the surface area of the graphene aerogel was evaluated using the Brunauer–Emmett–Teller (BET) method. The electrical conductivity of the graphene aerogels and graphene–PDMS composites was measured by a two-probe method. Copper wires were embedded and connected to the graphene aerogels with silver paste before infiltration with PDMS precursors, which enables a strong electrical contact between the copper wires and the graphene network and consequently a small contact resistance. The current–voltage ( $I$ – $V$ ) curves were then obtained by the linear sweep voltammetry (LSV) method using a PGSTAT302N Autolab electrochemical workstation (Metrohm).

To evaluate their organic solvent sensing ability, the as-prepared graphene–PDMS composites with the attached copper wires were connected to the electrochemical workstation, and a constant potential of 0.01 V was applied. Variations in the current passing through the graphene–PDMS composites were recorded when a fixed volume (5.0  $\mu$ L) of different solvents was applied on the surface of the graphene–PDMS composites. All the experiments were carried out at an ambient temperature ( $\sim 22$  °C).

## Results and discussion

In a typical preparation, OA and NaI were added to a GO suspension prepared using the modified Hummer's method, and after homogenization by sonication, the mixture was placed in an oil bath at 90 °C for 12 hours without stirring. As shown in Fig. 1a and b, the dark brown homogeneous mixture of GO (concentration 2.5 mg mL<sup>-1</sup>), OA, and NaI turned into a black free-standing macrostructure (denoted as hydrogel) after the reaction. After freeze-drying of the hydrogel, a graphene aerogel with low density ( $\sim 8.0$  mg cm<sup>-3</sup>) was obtained, as shown in Fig. 1c. The microscopic structure of the graphene aerogel was characterized by SEM measurements. As shown in Fig. 1d, the graphene aerogel exhibits 3D network structures, composed of a large amount of interconnected pores with the pore sizes of 3–5  $\mu$ m. As indicated in the magnified SEM image in Fig. 1e, the walls of these pores are thin, consisting of thin layers of stacked graphene nanosheets. The surface area of the graphene aerogel is 151 m<sup>2</sup> g<sup>-1</sup> obtained by fitting the isotherm using the BET method. The current *in situ* reduction-assembly method using the combination of OA and NaI as the reducing medium enables stable 3D graphene macrostructures to be readily prepared from various starting GO concentrations ranging from 0.1 to

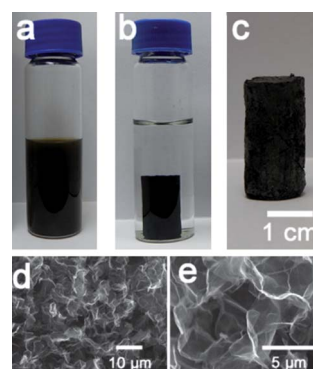
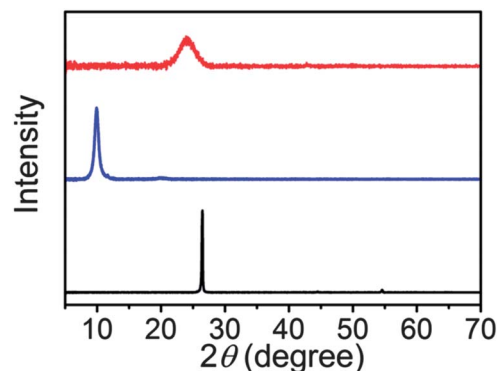


**Fig. 1** Photographs of the aqueous suspension of GO with OA and NaI before the reaction (a), graphene hydrogel after the reduction (b), freeze-dried aerogel (c). (d and e) SEM images of the freeze dried graphene aerogel with different magnifications.

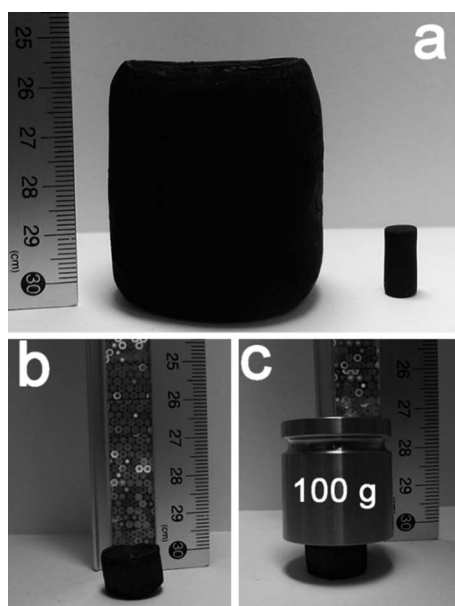
4.5 mg mL<sup>-1</sup> and the detailed reaction mechanisms will be discussed in later sections.

Fig. 2 shows the XRD patterns of the pristine graphite, GO, and the thus-prepared graphene aerogel. The XRD pattern of the GO exhibits a prominent peak at 9.85°, which corresponds to an interlayer spacing of 8.98 Å. In comparison, this peak completely disappears in the XRD pattern of the graphene aerogel, which instead exhibits a relatively broad peak at 24.1° corresponding to an interlayer spacing of 3.69 Å. The broad XRD peak of the graphene aerogel indicates the poor ordering of the graphene nanosheets along their stacking direction, and also reflects that the network of the aerogel is composed of few-layer stacked graphene sheets.<sup>26,31</sup>

One of the unique advantages of the current preparation method is that the volume of the thus-prepared graphene aerogels can be readily varied by varying the volume of the starting GO suspension with its concentration being constant. As exemplified in Fig. 3a, the graphene aerogels with significantly contrasting volumes could be prepared by simply employing different volumes (*e.g.*, of 300 mL and 1.5 mL) of the same GO suspension with other preparation conditions (*e.g.*, temperature, reaction duration, concentration of OA and NaI) being the same. The as-obtained monolithic graphene aerogel exhibits a good mechanical property. As shown in Fig. 3b and c a slice of the graphene aerogel prepared from 2.5 mg mL<sup>-1</sup> GO, with a weight



**Fig. 2** XRD patterns of graphite (black), GO (blue), and graphene aerogel prepared from 2.5 mg mL<sup>-1</sup> GO suspension (red).



**Fig. 3** (a) Photographs of the graphene aerogels prepared from 300 and 1.5 mL starting GO suspensions with the concentration of  $2.5 \text{ mg mL}^{-1}$ . (b and c) Photographs showing a graphene aerogel with a height of  $\sim 1 \text{ cm}$  can support a 100 g weight with little deformation.

of 13.5 mg and height of  $\sim 1.0 \text{ cm}$ , could support at least 100 g weight with little deformation, which is 7400 times the weight of the graphene aerogel.

Interestingly, it was found that when either NaI or OA alone, not both together, was added into the GO suspension, no regular monolithic 3D assemblies were formed under otherwise the same conditions and only discrete, piece-wise agglomerates were observed. This result clearly reveals the indispensability of the combination of NaI and OA for the successful preparation of the graphene macroscopic assemblies in the current system.

To clarify the roles of the co-presence of NaI and OA in obtaining the 3D macroscopic graphene assemblies in the current study, the products from the reactions of the GO with either NaI or OA alone, and the one with both together were collected and composition analyses of these products were carried out. Fig. 4a compares the FTIR spectra of the starting GO and the graphene aerogel prepared in the presence of OA and NaI together with the one of the GO reduced by either NaI or OA alone. The FTIR spectrum of the GO reveals the presence of a large amount of oxygen-containing groups, such as the strong and broad peak of

the hydroxyl group at around  $3400 \text{ cm}^{-1}$  and  $1401 \text{ cm}^{-1}$ , the epoxy group at  $1226 \text{ cm}^{-1}$ , the alkoxy group at  $1050 \text{ cm}^{-1}$ , and the carbonyl group at  $1726 \text{ cm}^{-1}$ .<sup>48,49</sup> The peak located at  $1633 \text{ cm}^{-1}$  is associated with aromatic C=C bonds in the GO.<sup>30,49</sup> The reduction of the GO by OA and NaI together led to a dramatic decrease or disappearance of the adsorption bands of these oxygen-containing functional groups on the graphene aerogel, indicating that the GO was reduced successfully. At the same time, after the reduction by OA and NaI together, a new peak at  $1565 \text{ cm}^{-1}$  appeared, which corresponds to the skeletal vibration of graphene and is believed to result from the restoration of the highly conjugated structure of graphene after the reduction.<sup>49</sup> In sharp contrast, the FTIR spectral features of the oxygen-containing groups largely remained for the GO reacted with either NaI or OA alone, indicating that the reduction of the GO by sole OA or NaI was not effective. It is worth mentioning that we found the 12 hour reduction time of the GO by the OA and NaI together was sufficient, and any further prolongation in the reduction time resulted in no obvious changes in the FTIR spectra of the graphene aerogels (ESI, Fig. S1†).

Raman spectroscopy is one of the most widely used techniques to characterize the structural and electronic conjugation of graphene materials.<sup>44–46,50,51</sup> As shown in Fig. 4b, all Raman spectra of the GO and the products of GO reacted with OA and/or NaI exhibit a prominent D band and G band. The G band of the GO was located at  $1595 \text{ cm}^{-1}$ , and after the reduction by OA and NaI together, the G band of the graphene aerogel thus-prepared shifted to  $1589 \text{ cm}^{-1}$ , which is due to the recovery of the hexagonal network of the carbon atoms with defects. For this sample, the intensity ratio of the D and G bands,  $I_D/I_G$ , increased dramatically from 0.99 for the GO to 1.54. In contrast, the  $I_D/I_G$  of the GO reacted with either NaI or OA alone changed little, being only 1.04 and 1.07. The increased  $I_D/I_G$  for the graphene aerogel is attributed to the increased number of isolated  $\text{sp}^2$  domains and again indicates the effectiveness of the GO reduction by the combination of OA and NaI in the current method.<sup>50,51</sup> Moreover, relative to the GO, the intensity of the 2D ( $2700 \text{ cm}^{-1}$ ) and S3 ( $2938 \text{ cm}^{-1}$ ) bands for the graphene aerogel increased greatly, which can be considered as a distinct proof of graphene formation.<sup>46</sup>

The improved reducing effect of GO by the combination of OA and NaI was also examined by X-ray photoelectron spectroscopy (XPS) measurements. Fig. 5 shows the C 1s spectra of GO and the products of GO reduced with OA and/or NaI. Before reduction, the C 1s spectrum of the GO (Fig. 5a) was fitted with four components, located at 284.4, 286.4, 287.9, and 288.9 eV corresponding to the C=C/C–C (aromatic ring), C–O–C/C–OH (epoxy and hydroxyl), C=O (carbonyl), and O=C–OH (carboxyl) groups, respectively.<sup>48,51</sup> Meanwhile, the dominant peak at 286.4 eV indicates that the most oxygen-containing functional groups in GO are hydroxyl and epoxy groups. After reaction of GO by NaI, OA, and combination of OA and NaI, an additional peak centered at 290.6 eV was required to fit the C 1s spectra of these samples. This peak corresponds to the  $\pi$ - $\pi^*$  shake-up satellite structure characteristic of conjugated systems.<sup>52</sup> After chemical reduction, we have observed that there is an increase in the intensity of  $\text{sp}^2$  hybridized carbon, in addition to the decrease of the intensity of hydroxyl and epoxy groups. The atomic ratio of O/C was estimated from the survey

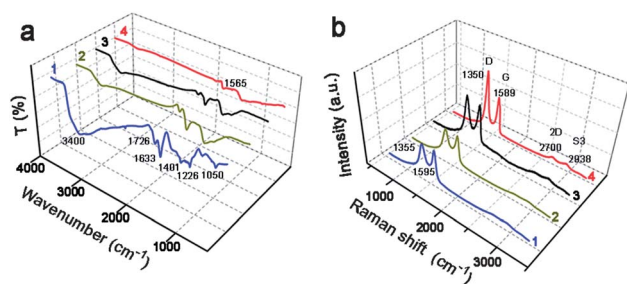


**Fig. 4** FTIR (a) and Raman (b) spectra of GO (1), GO reacted with NaI alone (2) and with OA alone (3), graphene aerogel (4).

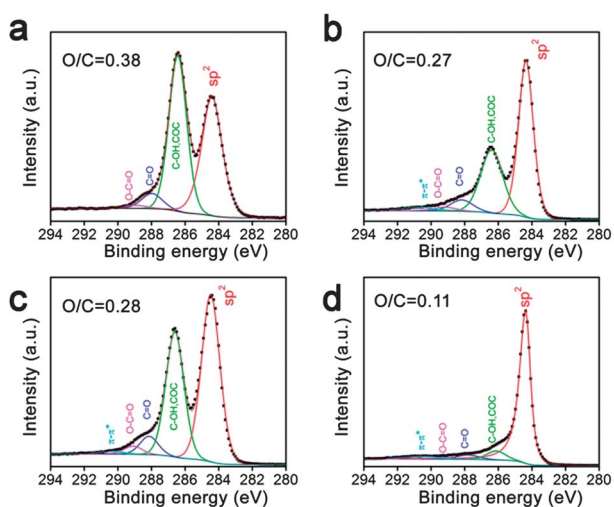
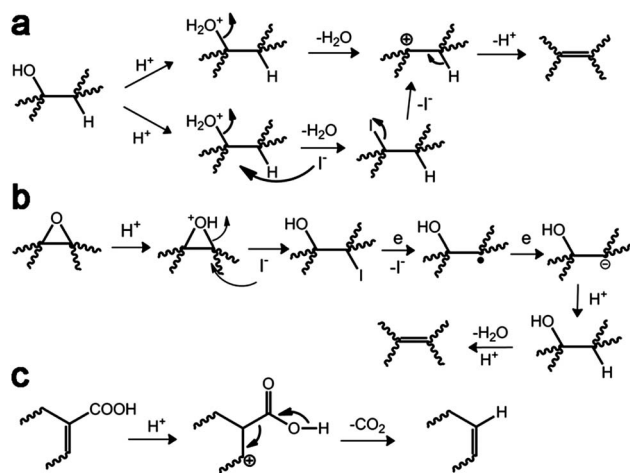


**Fig. 5** XPS spectra of GO (a), GO reacted with NaI alone (b) and with OA alone (c), graphene aerogel (d). The atomic ratios of O/C of these samples are 0.38, 0.27, 0.28, and 0.11, respectively.

spectra for these samples. The dramatic decrease of the O/C ratio of graphene aerogel prepared from the combination of OA and NaI also confirms the efficient removal of oxygen-containing functionalities.

From the above results, we can conclude that the combination of OA and NaI is crucial to sufficiently reduce the GO in the current system. Scheme 1 presents the proposed mechanisms for the reduction of GO by the combination of OA and NaI. The presence of OA provides abundant  $H^+$ , which greatly lowers the pH of the GO suspension (pH was measured to be  $\sim 0.7$ ), and such an acidic medium is favorable for  $I^-$  ions to catalyze the ring-opening reaction of epoxy groups, and to convert them into hydroxyl groups.<sup>45,46</sup> These hydroxyl groups undergo dehydration under acidic conditions to yield corresponding olefins. At the same time, the hydroxyl groups can also be substituted by iodine, and because of the low binding energy of C–I bonds, the substituted iodine atoms are expected to be easily eliminated,



**Scheme 1** Proposed mechanisms for the reduction of oxygen-containing groups such as hydroxyl (a), epoxy (b), and carboxyl (c) groups of the GO in the co-presence of OA and NaI.

leaving behind on the carbon lattice corresponding olefins.<sup>45</sup> It is known that the decarboxylation of carboxylic acids can be catalyzed by acid to yield olefins and such decarboxylation can be another potential pathway for the reduction of the GO to graphene in the current system due to the extended conjugation in the carbon framework in the GO, which is favorable for the decarboxylation.<sup>51,53</sup> Moreover, OA, as a reducing agent, can by itself release electrons during the reaction, which is also favorable for the reduction of the GO.<sup>49</sup>

During the reduction of the GO, the restored conjugated graphene structures facilitate the self-assembly of the reduced GO nanosheets due to the hydrophobic and  $\pi$ - $\pi$  interactions, and they themselves first agglomerate. With the reduction proceeding, the hydrophobicity and the  $\pi$ -conjugated structures of the reduced GO nanosheets further increases, which enhances the strength and degree of the nanosheets stacking and increases the number of the cross-linking sites where different nanosheets are joined together. As a result, the agglomerates of the reduced GO become more compact as the reduction goes on and a stable monolithic graphene assembly in the form of hydrogel is finally obtained at the end of the reaction.<sup>26,44</sup> In comparison, for the GO reacted with either OA or NaI alone, partial reduction of the GO occurs as revealed by the XPS and FTIR measurements, but the degree of the reduction is not sufficient to result in a compact stacking of the reduced GO to form a monolithic graphene assembly and instead only discrete and piece-wise black agglomerates are obtained (see ESI, Fig. S2†).

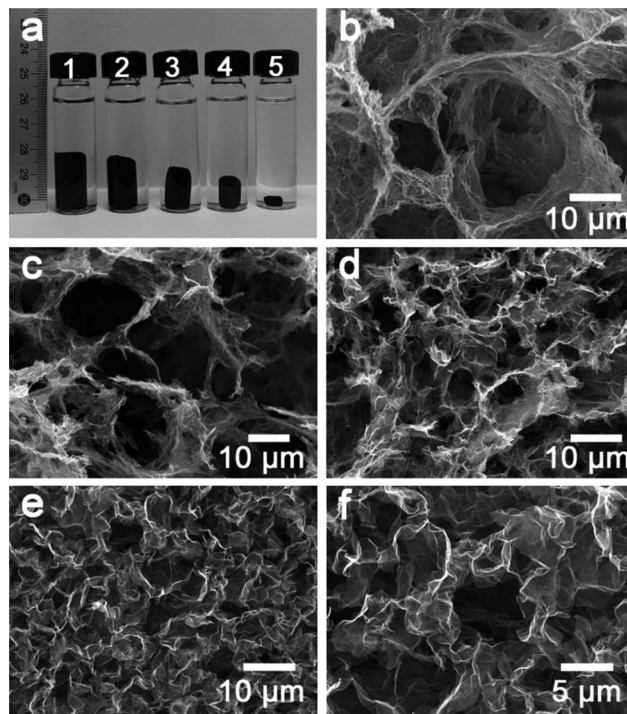


**Fig. 6** (a) Photograph showing the graphene hydrogels prepared from the GO suspension with concentrations of: (1) 4.5, (2) 2.5, (3) 1.0, (4) 0.5, and (5) 0.1  $mg\ mL^{-1}$ . SEM images of the graphene aerogels prepared from the GO suspensions with concentrations of (b) 0.1, (c) 0.5, (d) 1.0, and (e and f) 4.5  $mg\ mL^{-1}$  respectively. SEM images of graphene aerogels from 2.5  $mg\ mL^{-1}$  GO are given in Fig. 1d and e.

The current *in situ* reduction-assembly method using OA and NaI as the reducing agents allows for a wide concentration range of the GO to start with. Fig. 6a shows a photo of a series of the graphene hydrogels obtained from the GO suspensions with five different starting GO concentrations ranging from 0.1 to 4.5 mg mL<sup>-1</sup>. Clearly, all the GO suspensions successfully resulted in macroscopic assemblies (*i.e.*, hydrogels), with the volume of the hydrogels decreasing with decreasing starting GO concentrations. To the best of our knowledge, the GO concentration of 0.1 mg mL<sup>-1</sup> is the lowest GO concentration ever reported for preparation of a stable graphene assembly *via* an *in situ* reduction-assembly method. The possible explanations for the formation of the graphene hydrogels at low GO concentrations are offered as follows. First, as discussed earlier, the presence of the OA in the GO suspensions at all concentrations leads to a low pH (~0.7), which diminishes the electrostatic repulsions between individual GO nanosheets. Secondly, OA has two carboxyl groups and presumably it can act as a cross-linker between individual GO nanosheets *via* hydrogen-bonding which brings closer the starting GO nanosheets and leads to stable GO agglomerates. In the course of the GO reduction, as the reduced GO nanosheets further stack and cross-link due to the enhanced hydrophobic and  $\pi$ - $\pi$  interactions, the agglomerates join together and become more compact. Finally a stable graphene assembly is formed upon complete reduction of the GO even with the ultralow GO starting concentrations.

As shown in the SEM images in Fig. 6b–f, all the graphene aerogels, which were obtained by freeze drying the graphene hydrogels, exhibit similar 3D network structures composed of a large amount of interconnected macropores. Interestingly, it was found that the pore sizes of the graphene aerogels decreased with increasing GO starting concentrations (Table 1). Due to their highly macroporous structures, the graphene aerogels exhibited very low densities. For instance, the graphene aerogel prepared from a starting GO concentration of 4.5 mg mL<sup>-1</sup> had a density of 14.2 mg cm<sup>-3</sup>. As the GO starting concentrations decreased, the density of the resulted graphene aerogels decreased accordingly. Incidentally, the aerogels prepared from the starting GO concentrations  $\leq 1.0$  mg mL<sup>-1</sup> showed deteriorated mechanical strength, but as the GO concentration increased beyond 1.0 mg mL<sup>-1</sup> (specially, 2.5 and 4.5 mg mL<sup>-1</sup>), stable graphene aerogels with high mechanical strength were obtained as revealed in Fig. 3b and c. Supposedly this was due to improved crosslinking sites at high GO concentrations.

The reduction of the GO by OA and NaI restores the highly conjugated structure of graphene, which endows the as-resulted

graphene aerogels with electrically conducting properties. For instance, the graphene aerogel prepared from the starting GO concentration of 4.5 mg mL<sup>-1</sup> showed a bulk conductivity of 24.8 S m<sup>-1</sup>, which is highest among all the aerogels prepared in this study. The fact that the conductivity of the aerogels improved with increasing GO starting concentrations in this study can be explained by the improved interconnection (or crosslinking) of the graphene nanosheets in the bulk aerogels.

As an electrically conducting 3D network, graphene aerogel has been demonstrated to be very useful in many energy-related applications.<sup>26,31,35,36</sup> Besides, the highly macroporous structure of the graphene aerogels enables polymers to be readily infiltrated, leading to 3D graphene network-based electrically conducting composites.<sup>38</sup> As a proof of concept, in this study, polydimethylsiloxane (PDMS) was infiltrated into the 3D network of the graphene aerogel and the thus-prepared graphene–PDMS composite was demonstrated to be an effective organic-solvent-sensing device to differentiate solvents with different polarity. Such a device operates on a basis of swelling effect. Organic solvents cause the polymer to swell, which reduces the number of electrical conduction paths through the composite material, leading to an increase in the overall resistance of the composite material.<sup>54,55</sup> PDMS is known to swell in response to various organic solvents and the degree of its swelling is related to the polarity of the solvents, with the swelling degree increasing with decreasing solvent polarity.<sup>56,57</sup> Therefore, PDMS is a judicious choice of polymer for such a device.

To prepare such a device, a piece of the graphene aerogel (prepared from 2.5 mg mL<sup>-1</sup> GO) was attached to copper wires,

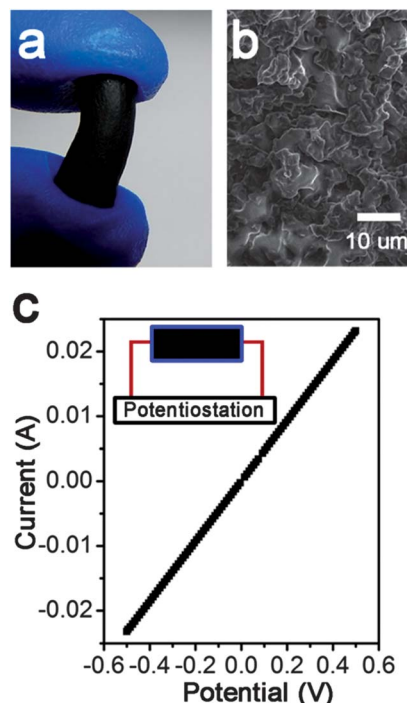


**Fig. 7** (a) Photograph of a bent graphene–PDMS composite, showing its good flexibility. (b) SEM image of the graphene–PDMS composite. (c) *I*–*V* curve of the graphene–PDMS composite exhibiting an Ohmic characteristic; inset shows a scheme of the system setup for the *I*–*V* curve and sensing measurements.

**Table 1** Physical properties and electrical conductivity of the graphene aerogels prepared from the GO with different starting concentrations

GO concentration (mg mL <sup>-1</sup> )	Average pore size <sup>a</sup> (μm)	Bulk density (mg cm <sup>-3</sup> )	Electrical conductivity (S m <sup>-1</sup> )
4.5	2.1 ± 0.4	14.2	24.8
2.5	3.1 ± 1.5	8.0	18.3
1.0	4.6 ± 1.3	4.5	7.3
0.5	15.9 ± 3.1	3.6	3.1
0.1	24.2 ± 3.5	2.2	0.7

<sup>a</sup> Determined from the SEM images.

and a PDMS precursor, containing the Sylgard 184 silicone elastomer base and curing agent, was subsequently infiltrated and then thermally cured. As shown in Fig. 7a, the prepared graphene–PDMS composite exhibited a good flexibility and could be bent and twisted without breaking. The SEM image in Fig. 7b revealed that the PDMS infiltrated in the void space of the graphene aerogel and that the graphene sheets adhered well to the PDMS polymer. The graphene–PDMS composite also showed a good electrically conducting property as shown in Fig. 7c, and the electrical conductivity showed no significant change after the PDMS infiltration, indicating that the introduction of the PDMS polymer did not degrade the interconnection of the graphene 3D network.

For the organic solvent sensing tests, a constant potential of 0.01 V was applied on the composite in all experiments, and the changes in the electrical current passing through the composite were monitored while solvents with different polarity were applied directly on the surface of the composite. Fig. 8 shows the real-time response (current *versus* time) of the sensor to the applied solvents of ethanol, acetone, and chloroform at ambient temperature. The response is calculated by dividing the recorded instant current by the initial current through the composite. After applying a droplet of the solvent onto the composite surface, the current signal through the PDMS–graphene composite decreased instantly (within several seconds),

indicating that the resistance of the composite-based sensor had increased due to the fast swelling of the PDMS. After the evaporation of the applied solvent, the current recovered to its initial value, and the response and recovery of the composite were completely reversible. Importantly, it can be found that as the polarity of the solvent decreased (the reported relative polarity of ethanol, acetone, and chloroform are 0.654, 0.355, and 0.259, respectively),<sup>58</sup> the changes in the current increased obviously, indicating that the PDMS–graphene composite can be potentially used for differentiating organic solvents with different polarity.

## Conclusions

In summary, we have developed a facile reduction-induced self-assembly method by using a novel combination of reducing agents OA and NaI for the one-step preparation of 3D graphene assemblies. We demonstrated that the highly porous graphene assemblies can be used as the matrix for the preparation of electrically conducting composites for the application of differentiating organic solvents with different polarity. We believe that the current method for the preparation of graphene macrostructures, owing to its simplicity, scalability, and environmental-friendliness, might be very useful for many other potential applications.

## Acknowledgements

The authors thank Prof. Dongyuan Zhao at Fudan University for his kind support and helpful discussion.

## Notes and references

- 1 K. S. Novoselov, A. K. Geim, S. V. Morozov, D. Jiang, Y. Zhang, S. V. Dubonos, I. V. Grigorieva and A. A. Firsov, *Science*, 2004, **306**, 666–669.
- 2 A. K. Geim and K. S. Novoselov, *Nat. Mater.*, 2007, **6**, 183–191.
- 3 A. A. Balandin, S. Ghosh, W. Z. Bao, I. Calizo, D. Teweldebrhan, F. Miao and C. N. Lau, *Nano Lett.*, 2008, **8**, 902–907.
- 4 C. Lee, X. D. Wei, J. W. Kysar and J. Hone, *Science*, 2008, **321**, 385–388.
- 5 C. N. R. Rao, A. K. Sood, K. S. Subrahmanyam and A. Govindaraj, *Angew. Chem., Int. Ed.*, 2009, **48**, 7752–7777.
- 6 X. Huang, Z. Y. Yin, S. X. Wu, X. Y. Qi, Q. Y. He, Q. C. Zhang, Q. Y. Yan, F. Boey and H. Zhang, *Small*, 2011, **7**, 1876–1902.
- 7 X. Huang, X. Y. Qi, F. Boey and H. Zhang, *Chem. Soc. Rev.*, 2012, **41**, 666–686.
- 8 X. Huang, Z. Y. Zeng, Z. X. Fan, J. Q. Liu and H. Zhang, *Adv. Mater.*, 2012, DOI: 10.1002/adma.201201587.
- 9 Q. Y. He, S. X. Wu, Z. Y. Yin and H. Zhang, *Chem. Sci.*, 2012, **3**, 1764–1772.
- 10 Y. X. Xu and G. Q. Shi, *J. Mater. Chem.*, 2011, **21**, 3311–3323.
- 11 S. Y. Yin, Z. Q. Niu and X. D. Chen, *Small*, 2012, **8**, 2458–2463.
- 12 Q. Ji, I. Honma, S. M. Paek, M. Akada, J. P. Hill, A. Vinu and K. Ariga, *Angew. Chem., Int. Ed.*, 2010, **49**, 9737–9739.
- 13 J. J. Yoo, K. Balakrishnan, J. Huang, V. Meunier, B. G. Sumpter, A. Srivastava, M. Conway, A. L. M. Reddy, J. Yu, R. Vajtai and P. M. Ajayan, *Nano Lett.*, 2011, **11**, 1423–1427.
- 14 H. L. Li, S. P. Pang, S. Wu, X. L. Feng, K. Müllen and C. Bubeck, *J. Am. Chem. Soc.*, 2011, **133**, 9423–9429.
- 15 J. F. Shen, Y. Z. Hu, C. Li, C. Qin, M. Shi and M. X. Ye, *Langmuir*, 2009, **25**, 6122–6128.
- 16 L. J. Cote, F. Kim and J. X. Huang, *J. Am. Chem. Soc.*, 2009, **131**, 1043–1049.
- 17 X. L. Li, G. Y. Zhang, X. D. Bai, X. M. Sun, X. R. Wang, E. G. Wang and H. J. Dai, *Nat. Nanotechnol.*, 2008, **3**, 538–542.

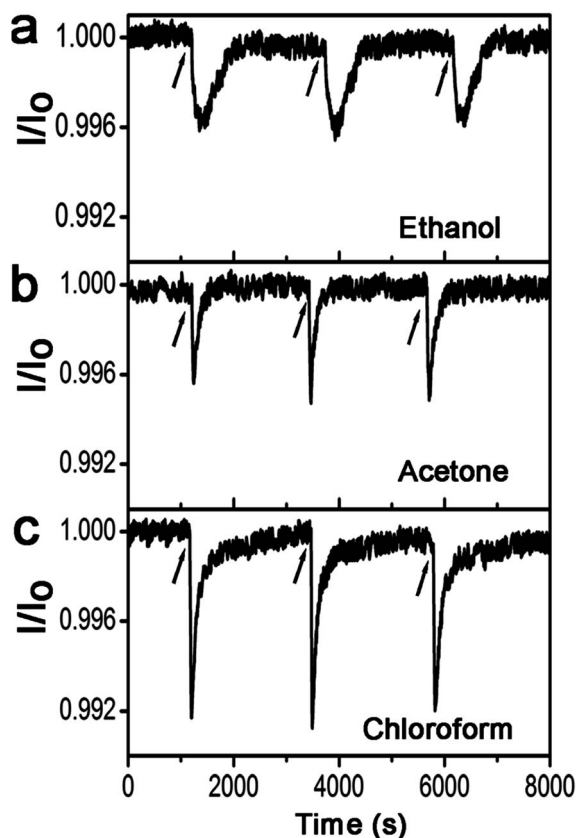


**Fig. 8** The real-time change of the current passing through the graphene–PDMS composite when solvents of ethanol (a), acetone (b), and chloroform (c) were applied onto its surface. The applied potential was fixed at 0.01 V. Arrows indicate the application of organic solvent droplets on the surface composite.

- 18 H. Q. Chen, M. B. Muller, K. J. Gilmore, G. G. Wallace and D. Li, *Adv. Mater.*, 2008, **20**, 3557–3561.
- 19 Y. X. Xu, H. Bai, G. W. Lu, C. Li and G. Q. Shi, *J. Am. Chem. Soc.*, 2008, **130**, 5856–5857.
- 20 S. J. Park, J. H. An, R. D. Piner, I. Jung, D. X. Yang, A. Velamakanni, S. T. Nguyen and R. S. Ruoff, *Chem. Mater.*, 2008, **20**, 6592–6594.
- 21 X. W. Yang, J. W. Zhu, L. Qiu and D. Li, *Adv. Mater.*, 2011, **23**, 2833–2838.
- 22 C. M. Chen, Q. H. Yang, Y. G. Yang, W. Lv, Y. F. Wen, P. X. Hou, M. Z. Wang and H. M. Cheng, *Adv. Mater.*, 2009, **21**, 3007–3011.
- 23 Y. W. Zhu, W. W. Cai, R. D. Piner, A. Velamakanni and R. S. Ruoff, *Appl. Phys. Lett.*, 2009, **95**, 103104.
- 24 J. P. Zhao, S. F. Pei, W. C. Ren, L. B. Gao and H. M. Cheng, *ACS Nano*, 2010, **4**, 5245–5252.
- 25 K. S. Kim, Y. Zhao, H. Jang, S. Y. Lee, J. M. Kim, K. S. Kim, J. H. Ahn, P. Kim, J. Y. Choi and B. H. Hong, *Nature*, 2009, **457**, 706–710.
- 26 Y. X. Xu, K. X. Sheng, C. Li and G. Q. Shi, *ACS Nano*, 2010, **4**, 4324–4330.
- 27 Z. H. Tang, S. L. Shen, J. Zhuang and X. Wang, *Angew. Chem., Int. Ed.*, 2010, **49**, 4603–4607.
- 28 H. Bai, K. X. Sheng, P. F. Zhang, C. Li and G. Q. Shi, *J. Mater. Chem.*, 2011, **21**, 18653–18658.
- 29 S. Z. Zu and B. H. Han, *J. Phys. Chem. C*, 2009, **113**, 13651–13657.
- 30 H. P. Cong, X. C. Ren, P. Wang and S. H. Yu, *ACS Nano*, 2012, **6**, 2693–2703.
- 31 X. T. Zhang, Z. Y. Sui, B. Xu, S. F. Yue, Y. J. Luo, W. C. Zhan and B. Liu, *J. Mater. Chem.*, 2011, **21**, 6494–6497.
- 32 J. L. Vickery, A. J. Patil and S. Mann, *Adv. Mater.*, 2009, **21**, 2180–2184.
- 33 M. A. Worsley, P. J. Pauzauskie, T. Y. Olson, J. Biener, J. H. Satcher and T. F. Baumann, *J. Am. Chem. Soc.*, 2010, **132**, 14067–14069.
- 34 Z. S. Wu, S. B. Yang, Y. Sun, K. Parvez, X. L. Feng and K. Müllen, *J. Am. Chem. Soc.*, 2012, **134**, 9082–9085.
- 35 S. Y. Yin, Y. Y. Zhang, J. H. Kong, C. J. Zou, C. M. Li, X. H. Lu, J. Ma, F. Y. C. Boey and X. Chen, *ACS Nano*, 2011, **5**, 3831–3838.
- 36 S. H. Lee, H. W. Kim, J. O. Hwang, W. J. Lee, J. Kwon, C. W. Bielawski, R. S. Ruoff and S. O. Kim, *Angew. Chem., Int. Ed.*, 2010, **49**, 10084–10088.
- 37 L. Estevez, A. Kelarakis, Q. M. Gong, E. H. Da'as and E. P. Giannelis, *J. Am. Chem. Soc.*, 2011, **133**, 6122–6125.
- 38 Z. P. Chen, W. C. Ren, L. B. Gao, B. L. Liu, S. F. Pei and H. M. Cheng, *Nat. Mater.*, 2011, **10**, 424–428.
- 39 Z. Q. Niu, J. Chen, H. H. Hng, J. Ma and X. D. Chen, *Adv. Mater.*, 2012, **24**, 4144–4150.
- 40 X. Jiang, Y. W. Ma, J. J. Li, Q. L. Fan and W. Huang, *J. Phys. Chem. C*, 2010, **114**, 22462–22465.
- 41 X. H. Cao, Y. M. Shi, W. H. Shi, G. Lu, X. Huang, Q. Y. Yan, Q. C. Zhang and H. Zhang, *Small*, 2011, **7**, 3163–3168.
- 42 X. C. Dong, H. Xu, X. W. Wang, Y. X. Huang, M. B. Chan-Park, H. Zhang, L. H. Wang, W. Huang and P. Chen, *ACS Nano*, 2012, **4**, 3206–3213.
- 43 X. C. Dong, X. W. Wang, L. H. Wang, H. Song, H. Zhang, W. Huang and P. Chen, *ACS Appl. Mater. Interfaces*, 2012, **4**, 3129–3133.
- 44 W. F. Chen and L. F. Yan, *Nanoscale*, 2011, **3**, 3132–3137.
- 45 S. F. Pei, J. P. Zhao, J. H. Du, W. C. Ren and H. M. Cheng, *Carbon*, 2010, **48**, 4466–4474.
- 46 I. K. Moon, J. H. Lee, R. S. Ruoff and H. Y. Lee, *Nat. Commun.*, 2010, **1**, 73.
- 47 W. S. Hummers and R. E. Offeman, *J. Am. Chem. Soc.*, 1958, **80**, 1339.
- 48 J. L. Zhang, H. J. Yang, G. X. Shen, P. Cheng, J. Y. Zhang and S. W. Guo, *Chem. Commun.*, 2010, **46**, 1112–1114.
- 49 P. Song, X. Y. Zhang, M. X. Sun, X. L. Cui and Y. H. Lin, *RSC Adv.*, 2012, **2**, 1168–1173.
- 50 S. Stankovich, D. A. Dikin, R. D. Piner, K. A. Kohlhaas, A. Kleinhammes, Y. Y. Jia, Y. Wu, S. T. Nguyen and R. S. Ruoff, *Carbon*, 2007, **45**, 1558–1565.
- 51 R. S. Dey, S. Hajra, R. K. Sahu, C. R. Raj and M. K. Panigrahi, *Chem. Commun.*, 2012, **48**, 1787–1789.
- 52 X. B. Fan, W. C. Peng, Y. Li, X. Y. Li, S. L. Wang, G. L. Zhang and F. B. Zhang, *Adv. Mater.*, 2008, **20**, 4490–4493.
- 53 W. S. Johnson and W. E. Heinz, *J. Am. Chem. Soc.*, 1949, **71**, 2913–2918.
- 54 C. A. L. Colard, R. A. Cave, N. Grossiord, J. A. Covington and S. A. F. Bon, *Adv. Mater.*, 2009, **21**, 2894–2898.
- 55 J. H. Zou, J. H. Liu, A. J. Karakoti, A. Kumar, D. H. Joung, Q. Li, S. I. Khondaker, S. Seal and L. Zhai, *ACS Nano*, 2010, **4**, 7293–7302.
- 56 J. N. Lee, C. Park and G. M. Whitesides, *Anal. Chem.*, 2003, **75**, 6544–6554.
- 57 I. Yoon, K. Kim, S. E. Baker, D. Heineck, S. C. Esener and D. J. Sirbully, *Nano Lett.*, 2012, **12**, 1905–1911.
- 58 R. Christian, *Solvents and Solvent Effects in Organic Chemistry*, Wiley-VCH, Weinheim, Germany, 3rd edn, 2002.